

Vibration Damping of Carbon Nanotube Assembly Materials

Jingna Zhao,¹ Fulin Wang,¹ Xin Zhang,¹ Linjie Liang,¹ Xueqin Yang,¹ Qingwen Li,¹ and Xiaohua Zhang^{1, a)}

*Division of Advanced Nano-Materials, Suzhou Institute of Nano-Tech and Nano-Bionics,
Chinese Academy of Sciences, Suzhou 215123, China*

Vibration reduction is of great importance in various engineering applications, and a material that exhibits good vibration damping along with high strength and modulus has become more and more vital. Owing to the superior mechanical property of carbon nanotube (CNT), new types of vibration damping material can be developed. This paper presents recent advancements, including our progresses, in the development of high-damping macroscopic CNT assembly materials, such as forests, gels, films, and fibers. In these assemblies, structural deformation of CNTs, zipping and unzipping at CNT connection nodes, strengthening and welding of the nodes, and sliding between CNTs or CNT bundles are playing important roles in determining the viscoelasticity, and elasticity as well. Towards the damping enhancement, strategies for micro-structure and interface design are also discussed.

I. INTRODUCTION

Vibrations are of concern to structural materials for the safety and comfort of civil infrastructures. For example, passenger comfort or the ride quality in aircraft and automobile is greatly affected by the vibrations caused by outside disturbances, such as aeroelastic effects and rough road surfaces. In other cases, civil engineering structures located in environments where earthquakes or large wind forces are common will be subjected to serious vibrations. Furthermore, vibration also affects the tracking and pointing characteristics and accuracy of weapon systems mounted on aircraft and land systems. Unfortunately, most of the materials are inherently poor in vibration reduction.^{1–4} A material that exhibits good vibration reduction along with high specific stiffness/modulus and strength becomes very vital for everyday life. Vibration reduction is usually reflected by the damping capacity, which describes how much mechanical energy can be dissipated during the vibration. Damping of a structure can be attained by passive or active methods.¹ The passive methods depend on the inherent ability of certain materials to absorb the vibrational energy, while the active methods make use of sensors and actuators to attain vibration sensing and activation to suppress the vibration in real time.

Metals and polymers are dominantly good materials for vibration damping, owing to their inherent viscoelasticity. Other mechanisms, especially structural defects such as dislocations, phase boundaries, grain boundaries, and various interfaces can also contribute greatly to damping. For composite structures, the overall damping capacity greatly depends on the reinforcement used and is proportional to the individual damping capacities of the reinforcement.⁵ Therefore, the microstructure design and interface control have become the most efficient ways to improve the damping performance.^{6–9}

Carbon nanotubes (CNTs), with their exceptional mechanical, electrical, and thermal properties, could be

building blocks for various macroscopic structural materials (architectures), such as one-dimensional (1D) fibers, 2D films and buckypapers, and 3D forests, gels, and sponges.^{10–16} These CNT-based materials have shown great potentials for civil, military, and aerospace applications. Different from metals and polymers, the CNT assembly materials possess rich contacts, connections, cross-links, and thus different types of interfaces between the nano components. For example, zipping/unzipping of adjacent CNTs, sliding between CNTs or CNT bundles, buckling of CNTs, and self-organization upon loading have become the main sources of viscoelasticity for the assembly materials.^{17–23}

Here, we review recent progresses on the damping performance of various CNT assembly materials, and report our studies on the dynamic properties of CNT fibers and films along with their related strengthening and toughening strategies. First, the basic concepts of viscoelasticity are provided in Sec. II. Then, the major progress report is organized in Sec. III according to the assembly way of the macroscopic CNT materials, namely CNT forests, gels, films and buckypapers, and fibers. Finally, a brief discussion on the strategies to build high-damping assemblies is given in Sec. IV.

II. BASIC CONCEPTS OF VISCOELASTICITY

Elasticity deals with elastic stresses and strains, their relationship, and the external forces that cause them.^{24,25} For all solid materials there is a domain in stress space in which strains are reversible due to small relative movements of atoms. Thus, the classical Hooke's law of elasticity applies. In reality, all materials deviate from Hooke's law in various ways, usually by exhibiting both viscous-like and elastic characteristics when undergoing deformation.^{25,26} Therefore, viscoelasticity considers in addition a dissipative phenomenon due to "internal friction", such as between molecules in polymers, between cells in wood, or between nanoparticles and matrix in nanocomposites.²⁷ It describes the ability of a material to both dissipate energy (viscous) and reversibly deform (elastic). The capacity of a system to dissipate dynamic

^{a)} Electronic mail: xhzhang2009@sinano.ac.cn

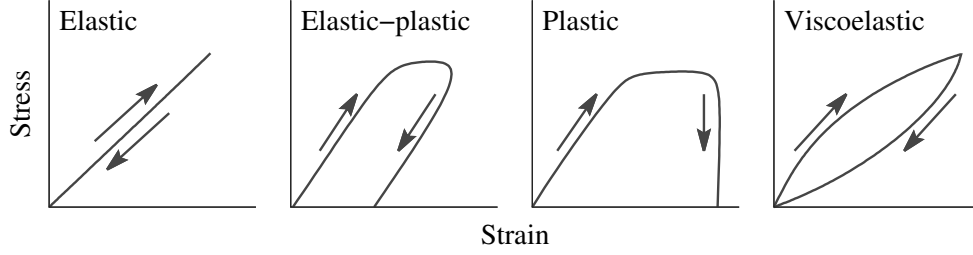


FIG. 1. Stress-strain curves illustrating different types of tensile behavior, of the elastic, elastic-plastic, plastic, and viscoelastic materials, respectively.

(vibration) energy is primarily described or measured by “damping”, either by energy dissipation or by a force that works to dissipate energy.

It is necessary to point out that viscoelasticity is not plasticity, with which it is often confused. A viscoelastic material will return to the original shape when the deforming force is removed, despite the fact that it might take a long time for the recovery. On the contrary, a plastic material can not recover after the load is removed. **Figure 1** schematically compares the stress-strain curves for different types of tensile behavior. For viscoelastic materials, although the original shape is recovered on removal of the load, some permanent deformation remains owing to plastic deformation or molecular slippage of an irreversible nature.

Two major types of experiment are performed on viscoelastic materials: transient and dynamic. Transient experiments involve deforming the material and studying the response of the material with time. Creep and stress-relaxation experiments are two transient experiments. In the dynamic tests, either stress or strain is varied cyclically with time, and the response is measured at various different frequencies of deformation.

A. Creep-Recovery and Stress Relaxation

Viscoelastic behavior manifests itself in creep and in stress relaxation. Creep is a progressive deformation of a material under constant stress, and, vice versa, stress relaxation is the gradual decrease of stress when the material is held at constant strain. Therefore, creep testing involves loading a sample with a set weight and watching the strain change over time, and recovery tests look at how the material relaxes once the load is removed. For stress relaxation, a sample is held at a set length and the force it generates is measured. Creep and creep-recovery tests are very useful for studying materials under very low shear rates or frequencies, under long test times, or under real use conditions.

In order to model the creep-recovery behavior, different combinations of springs (elastic sections) and dashpots (viscous sections) are suggested. For example, the Maxwell model with the spring and dashpot in series,

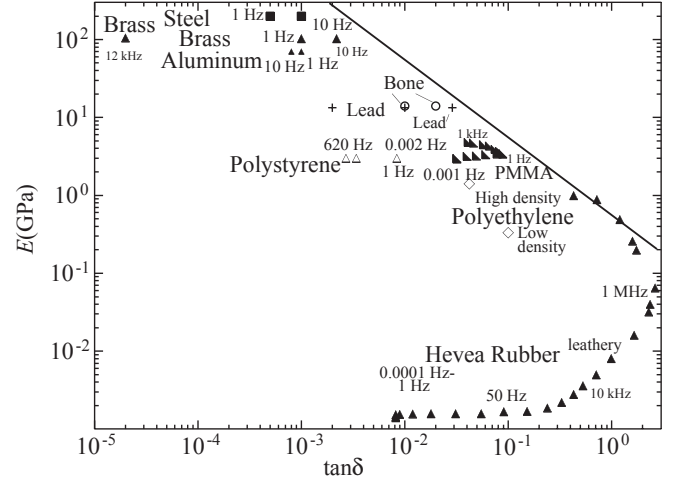


FIG. 2. Stiffness-loss map for some materials at near room temperature.²⁶ The diagonal line represents $E'' = E' \tan \delta = 0.6$ GPa. Most materials occupy the region to the left of that line.

and the Kelvin-Voigt model with the spring and dash-pot in parallel describe totally different creep-recovery behaviors.

B. Dynamic Mechanical Analysis

Viscoelasticity is widely studied using dynamic mechanical analysis (DMA) where an oscillatory force (stress) is applied to a material and the resulting displacement (strain) is measured. Under a sinusoidally varying stress $\sigma = \sigma_0 \sin \omega t$ where ω is the angular frequency, the strain ε is given by $\varepsilon = \varepsilon_0 \sin \omega t$ for elastic solids. For materials that exhibit damping, the stress and strain are not in phase; the strain lags behind the stress by a phase angle δ , which defines an in-phase and out-of-phase component of the stress, $\sigma' = \sigma_0 \cos \delta$ and $\sigma'' = \sigma_0 \sin \delta$. Therefore, a complex modulus, $E^* = E' + iE''$, is used to describe the stress-to-strain ratio, where $E' = \sigma'/\varepsilon_0 = |E^*| \cos \delta$ and $E'' = \sigma''/\varepsilon_0 = |E^*| \sin \delta$ are the storage modulus and loss modulus. A further quantity of vis-

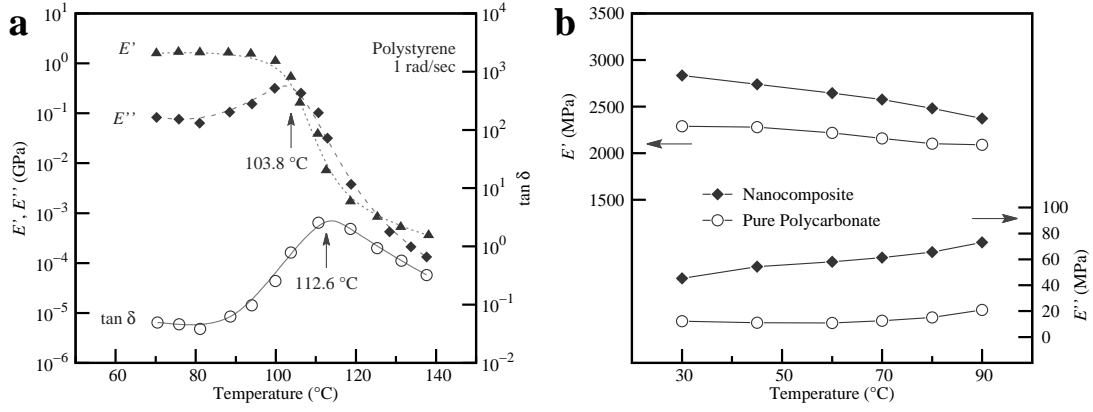


FIG. 3. (a) DMA thermal curves for PS film, step heating with isothermal frequency sweep every 5 °C in nitrogen.²⁸ (b) Storage modulus and loss modulus as functions of test temperature for constant strain amplitude (0.35%), at 1 Hz, for the pure polycarbonate and the nanocomposite samples containing 1.5 wt% of SWCNTs.²⁹

coelastic materials is the loss tangent, $\tan \delta = E''/E'$, where the ratio of the two modulus quantities represents an extremely useful damping quantity.

C. Common Viscoelastic Materials

Figure 2 provides a comparison of different viscoelastic materials in their stiffness-loss map.²⁶ Some single crystal materials exhibit the lowest losses, such as fused silica and sapphire, followed by common metals. Polymers in the transition region exhibit the highest losses commonly found in solids; the loss tangent can exceed unity. For common materials, high stiffness is associated with low loss, as reflected by the diagonal line as the upper limit for the loss modulus (Figure 2). (For more and detailed information, see Chapter 7 in R. Lakes, *Viscoelastic Materials*, 2009.²⁶)

Figure 3a shows a typical DMA result in temperature sweep mode for polystyrene (PS).²⁸ Generally, at the glass transition temperature, T_g , E' begins to decrease, while E'' and $\tan \delta$ go through maxima, as the temperature is increased. Notice that, different values of T_g can be defined, by using either the temperature of the loss modulus peak or the temperature of the $\tan \delta$ peak.

In order to improve the resilience and strength of polymers, extensive use of different types of filler materials have been considered. Nanometer-size fillers having large surface areas, such as nanotubes, nanorods, and nanofibers, have added advantages with greater interactions at the interfaces.^{3,29–37} For example, the introduction of single-walled CNTs (SWCNTs) into polycarbonate can activate interfacial slip at the tube-polymer interfaces at relatively low dynamic strain levels, by raising temperature to ~ 90 °C, and thus enhance the damping performance for vibration and acoustic suppression.²⁹ As shown in Figure 3b, after loading CNTs, the loss modulus increases much greater than the storage modulus.

III. VIBRATION DAMPING IN CARBON NANOTUBE ASSEMBLIES

Recent studies have shown that CNTs are ideal scaffolds to design and architect high-performance composites, at high CNT volume fractions or even fully composed by CNTs themselves.¹⁴ For example, the aligned pure or neat CNT films can exhibit a tensile strength and Young's modulus of 3.2 GPa and 172 GPa,^{38–40} and the high-volume-fraction CNT/bismaleimide (BMI) composites can be even as strong as 3.8–6.94 GPa in strength.^{41–44} In these high-strength materials, the CNTs should be highly packed and super aligned. Generally, these high-strength or high-stiffness CNT assembly materials show low loss tangent in dynamic tests. On the contrary, the loosely assembled macroscopic CNT materials, especially CNT forests, aerogels, and sponges, are naturally high-performance damping materials,^{18,20,23,45–49} owing to the sliding, zipping/unzipping, buckling, and cross-linking between/of the CNTs.^{17–23,50} Here, to provide a detailed and systematic overview of the various CNT assembly materials, recent progresses are discussed according to the assembly way for CNTs.

A. CNT Forests

CNT forests, also called vertically aligned CNTs or CNT arrays, have drawn considerable interest for a large range of potential applications, such as field emission electron sources, thermal interface materials, black body, composites, and CNT fibers.^{52–55} Notice that, for most cases, the forests are composed of multi-walled CNTs (MWCNTs), and for better mechanical performances, few-walled CNTs (wall number 2–4) are preferred.^{56,57} Due to the empty spaces between the aligned CNTs, as reflected by the low number density of 80–160 μm^{-2} or mass density of 1–90 $\mu\text{g mm}^{-3}$,^{17,47,58} the CNTs can easily bend upon compression or indentation. Thus, such as-

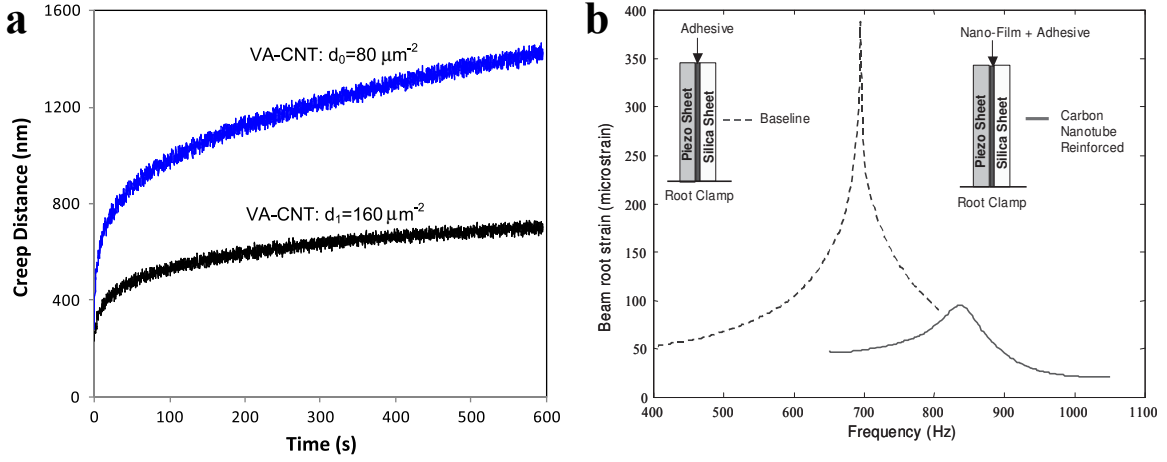


FIG. 4. (a) The indentation displacement-time curves of CNT forests with a low and high number density.⁴⁷ (b) Comparison of the dynamic response of the baseline beam and the CNT-reinforced sandwich beam for a frequency-sweep test at 50 V.⁵¹

sembly exhibits typical viscoelastic creep behavior, that is, when the indentation stress is increased and then held at a constant value, the indenter continues to penetrate into the specimen.⁴⁷ As shown in **Figure 4a**, a denser CNT forest has fewer geometric freedoms for the tube movement, and thus less creep deformation. However, due to the lack of cross-linking and interconnection between CNTs, such CNT forests still show strong compressive plasticity.^{46,47}

A more detailed study showed that the energy dissipation ability of CNT forests can be remarkably reduced by introducing solvents between the CNTs.⁵⁹ For example, water can induce a transition from the viscoelastic behavior into an elastic one, as hydration mediates the interaction between CNTs and thus reduces the frictional dissipation during the loading-unloading process. Further removal of water molecules allows the CNT forest to recover its viscoelastic behavior. Decane shows stronger ability to reduce the dissipation, indicating that the choice of solution is important to tune the viscoelasticity.

However, as CNT forests are loosely assembled and thus have weak mechanical performances in stretching, compressing, and bending, the most possible application of CNT forest is the structural damping enhancement. To do so, a piezo-silica sandwich beam has been embedded with a CNT forest, by stacking the CNTs in between a top piezoelectric sheet and a bottom silica substrate.⁵¹ Figure 4b compares the dynamic response of the sandwich beam with the baseline beam (without CNT reinforcement) for a frequency sweep test, at the same beam size. Clearly the CNT reinforcement has resulted in a very significant increase in the damping as well as the stiffness; the increased damping is reflected by the reduced dynamic amplification at resonance while the increased stiffness is manifested as a shift in the first bending frequency from ~ 700 Hz to ~ 840 Hz.

Another similar sandwich composites with improved

energy dissipation and damping properties were fabricated by stacking the freestanding CNT forests and carbon fiber fabrics, with a following epoxy infiltration using a vacuum-assisted resin transfer mold.⁶⁰ As compared to the conventional carbon fiber/epoxy laminate composites, the sandwich composites exhibit higher flexural rigidity and damping, which is achieved due to the rich interfacial areas inside the nanocomposites and the high thermal conductivity of CNTs.

In a following study where the silicon wafer covered with a CNT forest was tested, the mechanism for the enhanced damping was discussed. The primary energy dissipation is also believed to be a general result of the interfacial friction between individual CNTs, caused by their entanglements under cyclic deformation.⁶¹

Nowadays, CNT forests have been widely and successfully applied to enhance the damping performance of SiC fiber cloth,⁶² woven fiber-glass composites,⁶³ metal layers,⁶⁴ amorphous diamond film,⁶⁵ and polymer matrix.^{66,67}

B. CNT Gels

Besides such effect of intertube friction, the CNT entanglement plays more important roles in determining the viscoelasticity. (Even in CNT forests, the effect of entanglement is still non-negligible.⁶¹) This is because the entanglement can cause stronger intertube interaction than the alignment upon the structural deformation on CNT assemblies.

In one such assembly, as a result of water-assisted chemical vapor deposition (CVD) and a post-treatment of compression, each CNT makes contacts with numerous other CNTs, see the photograph and scanning electron microscopy (SEM) image in **Figure 5a**.¹⁸ (Such material is also called a gel, aerogel, or sponge, due to the feature of entanglement and the small mass density of 36

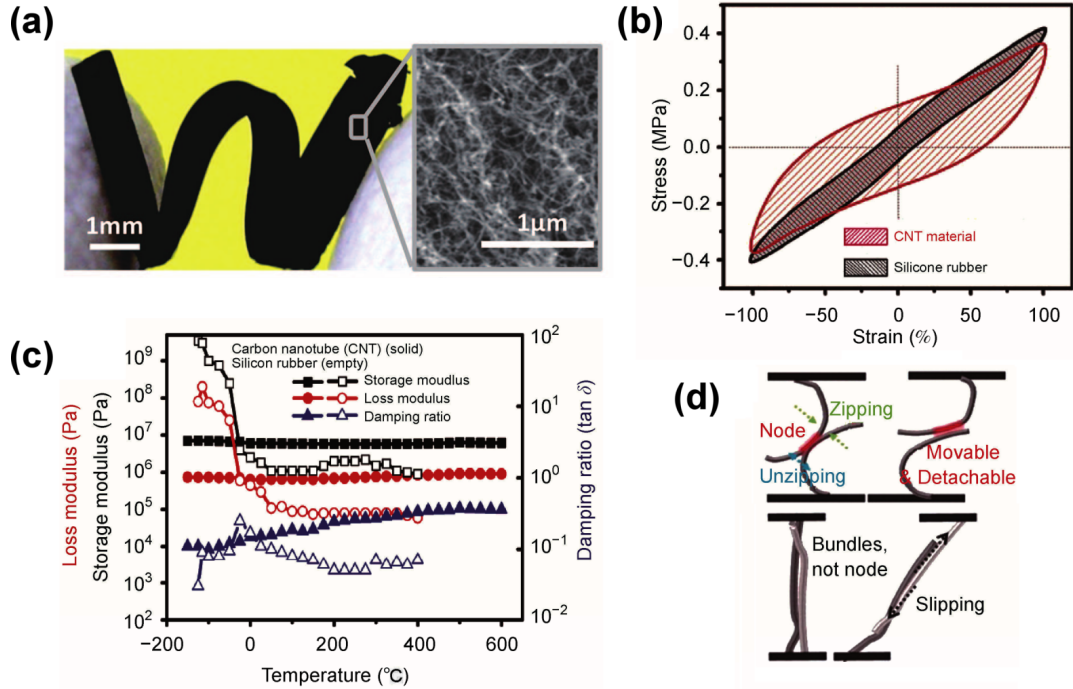


FIG. 5. Viscoelasticity of densified CNT gels.¹⁸ (a) Photograph and SEM image of the CNT gel. (b) Stress-strain curves of CNT gel and silicone rubber. (c) Temperature dependence of the storage modulus, loss modulus, and damping ratio of the CNT material, compared with silicone rubber. (d) Schematic of the zipping and unzipping of CNT connections nodes, as compared to the sliding between CNTs.

mg cm⁻³.) The stress-strain behavior from shear-mode DMA showed a strain up to 100%, high nonlinearity, and a closed hysteresis without abrupt changes, which are typical of viscoelastic, energy-dissipative, and highly deformable materials (Figure 5b). As compared to silicone rubber, the CNT gel had a larger enclosed area of the hysteresis loop, corresponding to a higher damping ratio ($E''/E' \approx 0.3$) at room temperature. (Notice that, such damping ratio was nearly constant in the frequency range of 0.1–100 Hz.) Interestingly, the viscoelastic properties measured in ambient N₂ were nearly constant over an exceptionally wide temperature range (from -140 to 600 °C) in contrast to the rubber, which showed large variation due to hardening (at -55 °C) and degradation (at 300 °C), see Figure 5c. Actually, due to the high thermal stability of CNT, the viscoelasticity could be unvaried beyond the limitation at -190 and >900 °C. Besides the damping ratio, the creep and creep recovery of CNT gels are also found to be at the same level as silicone rubber, still with an extreme temperature stability.⁶⁸ Furthermore, with increasing the gel's mass density, from 3.3 to 54 mg cm⁻³, both the storage modulus and damping ratio concurrently increased.⁶⁹

In the CNT gel, each CNT makes contact with numerous other tubes, resulting in a high density of connections (nodes). These nodes are separated mainly by isolated CNTs or CNT bundles (struts). Such intertube assembly of struts and nodes should be the key for structural cohe-

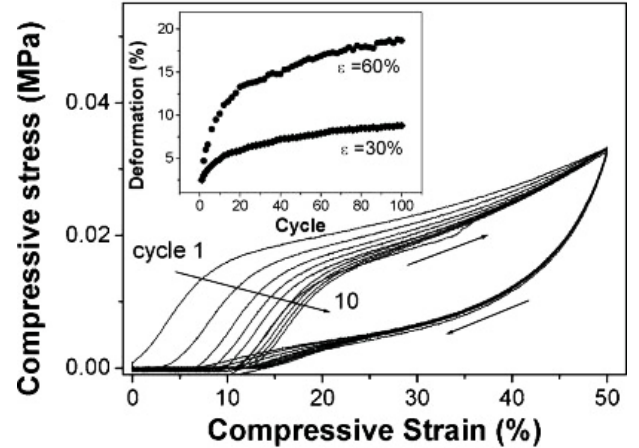


FIG. 6. Cyclic stress-strain curves at a maximum of 50% in air.⁷⁰ Inset, recorded deformations developed by compression for 100 cycles at different set strains of 30% and 60%, respectively.

siveness that allows for large deformations.^{18,70} It is also believed that the CNTs in a node can reversibly attach and detach through zipping and unzipping (Figure 5d). This process can dissipate energy because it overcomes the large van der Waals (vdW) attraction between CNTs when unzipping, yet no energy is required for zipping. On the contrary, when there is a lack of such connection

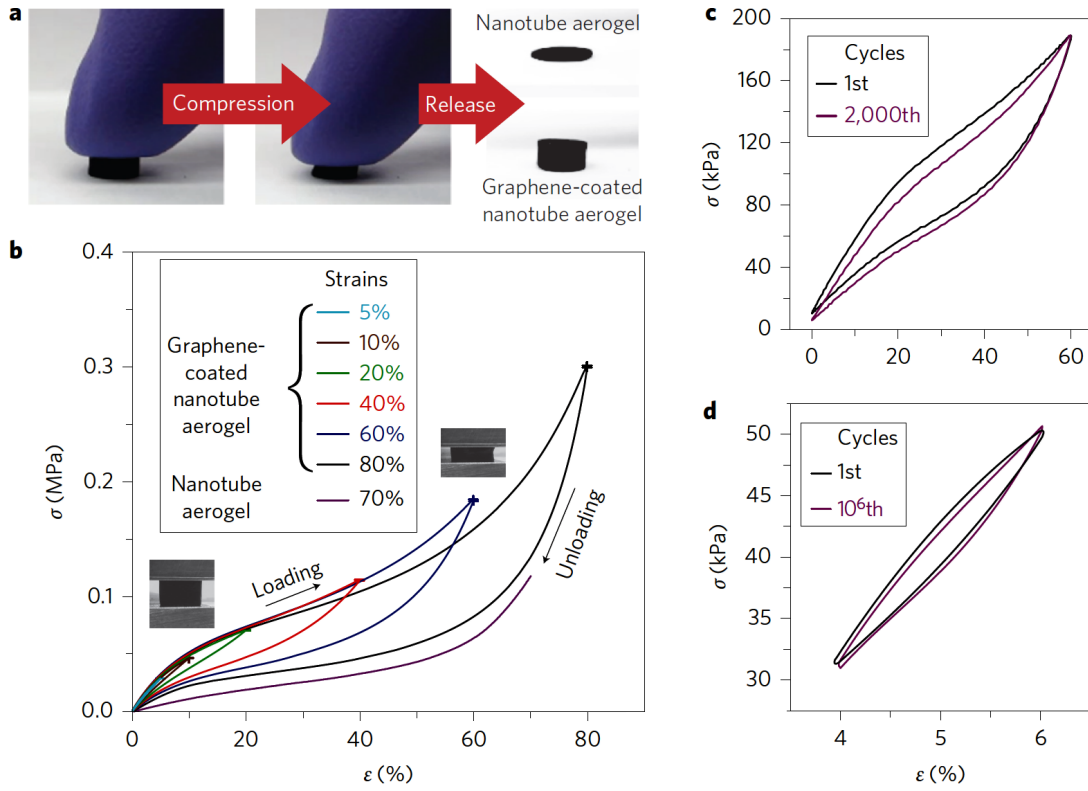


FIG. 7. Mechanical properties of CNT gels.⁷¹ (a) CNT gels collapse and graphene-coated CNT gels recover their original shape after compression by $>90\%$. (b) Stress-strain curves for CNT gels along the loading direction and for graphene-coated CNT gels during loading-unloading cycles. (c,d) Fatigue resistance of graphene-coated CNT aerogel at 60% strain, 1 Hz, for the 1st and 2,000th cycles (c) and at 2% strain, 100 Hz, for the 1st and 10⁶th cycles (d).

nodes, sliding between CNTs dominates the structural deformation for the gel. However, the sliding can not contribute much to the dissipation due to the small friction coefficient, and such sliding is rather a plastic and irreversible process.

Besides the CVD-based manufacture,^{18,70,72,73} CNT gels are also created by critical-point drying of solution-processed hydrogels,^{74–77} dry stacking of aligned CNT sheets drawn out from CNT forests,⁷⁸ and a frit compression method where surfactants or surface modification of CNT are avoided.^{79,80} However, these pristine CNT gels could collapse (irreversible thickness reduction for the CNT film) upon compressing, as shown in **Figure 6**, corresponding to a plastic deformation.⁷⁰ Therefore, various post-treatments have been proposed to improve the elasticity.

For example, by infiltrating pre-formed CNT gels with a low molecular-weight polyacrylonitrile (PAN) polymer and then critical-point drying, a PAN/CNT composite gel can be obtained. After degassing at 140 °C, stabilizing at 210 °C, and pyrolyzing at 1010 °C, these gels can be converted into graphene-coated gels, with the mass density increased from 8.8 to 14.0 mg cm⁻³.^{71,81} The pure CNT gels usually collapse upon high compression ratio, e.g., $>90\%$, while the graphene-coated gels can well recover their original shape (**Figure 7a**). Typ-

ical viscoelastic behaviors are observed in the plots of compressive stress σ versus compressive strain ϵ (Figure 7b). The energy dissipation, the hysteresis loop in the loading-unloading cycle, was negligible at a small strain of $\epsilon = 5\%$, but steadily increased with ϵ . Of great importance, after 2000 loading-unloading cycles at $\epsilon = 60\%$ and 1 Hz, and 1×10^6 cycles at $\epsilon = 2\%$ and 100 Hz, no significant plastic deformation or degradation in compressive strength is observed, corresponding to a high structural robustness (Figure 7c and d). Obviously, the graphene coating can modify the intertube interactions at the CNT connections, making them slippery and deformable into robust and elastic.

Similarly, the weak connections can be strengthened by joint-welding with a post CVD treatment.⁷³ The raw CNT gel was obtained by stacking up the continuous CNT networks grown via an injection CVD (iCVD), also called a floating catalyst CVD.^{44,82–85} The raw gel showed a low density of 1.78 mg cm⁻³, and could not recover the original shape even upon slight compressing. To improve the elasticity, a second CVD process was performed to fix the connection nodes in the 3D CNT networks. By tuning the treatment time for the post CVD, the gel's density increased up to 4 and 12.75 mg cm⁻³ after 2- and 4-h treatments, respectively. The CNTs in the untreated gel were free to slide with each other upon

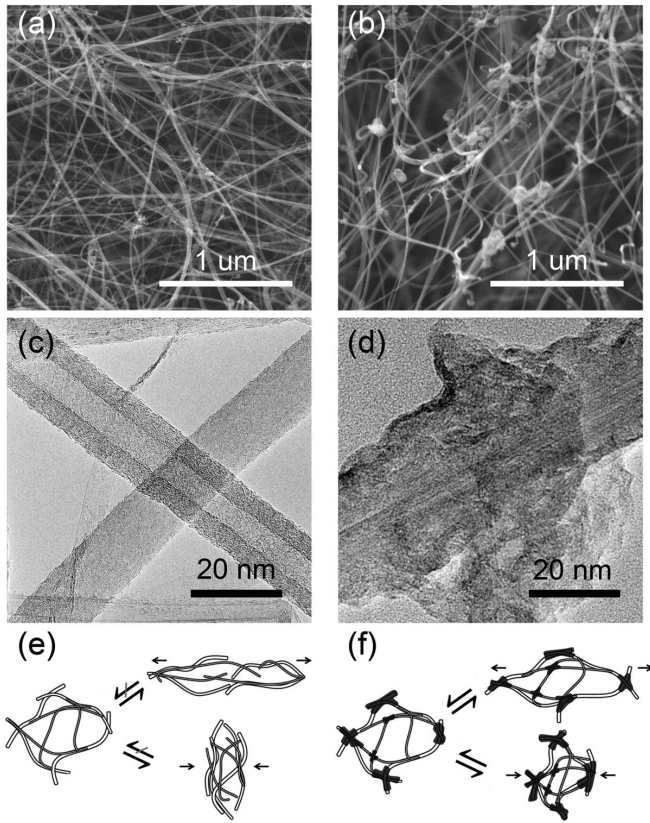


FIG. 8. Structural comparison between the CNT gels before and after joint welding: (a,b) SEM images, (c,d) TEM images, and (e,f) schematics of network deformation under stretching and compressing.⁷³

stretching and compressing, resulting in an irreversible plastic deformation. After the treatment, amorphous carbon was deposited at the nodes, effectively welding the CNT connections, as shown in **Figure 8a–d**. As a result, the post-treated gels became more and more elastic and could fully recover upon release from a compressive strain of 98%. Due to the increased elasticity, the compressive loss tangent at 1 Hz gradually decreased from ~ 0.09 to ~ 0.04 after a treatment time of 3 h.

For these CNT gels, temperature-invariant viscoelasticity has become a common feature,^{18,68,73,81} different from traditional viscoelastic polymers which degrade in performance at elevated temperatures. This is because CNTs can withstand high temperatures without any significant degradation.⁵¹ Typically, oxidation of MWCNTs in air begins at 600 °C. The porous nature of CNT gel also allows for rapid and efficient heat dissipation, which prevents significant heat accumulation. Further, the thermal stability of CNT gel depends on the contents of catalyst particles. The viscoelasticity can be unvaried up to 1200 °C for pure CNT gels while the existence of catalyst materials significantly hinders the up limit to just ~ 400 °C.¹⁸

Besides the experimental studies described above, several molecular dynamics (MD) simulations have been re-

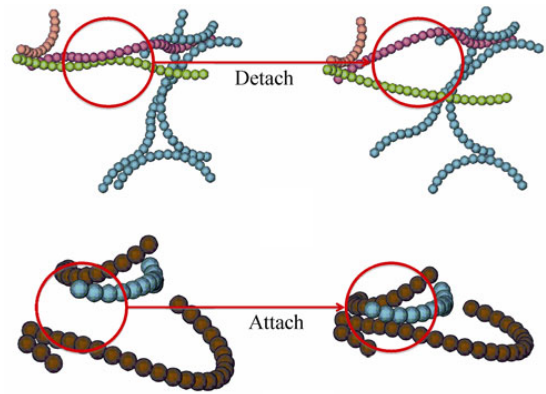


FIG. 9. Sudden detachment and attachment of individual CNTs during the loading process, which transforms elastic energy into heat.⁸⁸

ported to understand the dissipation mechanism in CNT gels.^{50,86–90} These studies can provide us an in-depth understanding of the viscoelasticity.

Zippering and unzipping have been confirmed by a coarse-grained MD study.⁵⁰ In the coarse-grained model, each CNT is mapped as a multi-bead chain. The intra-chain elasticity is described by a bond stretching and a bond angle bending term, reproducing the tube's modulus and bending rigidity. The inter-chain binding is captured by a Lennard-Jones type pair interaction between the coarse-grained beads. Simulations revealed that the temperature- and frequency-invariant hysteresis of CNT gels¹⁸ is due to unstable detachments/attachments of individual CNTs in the system induced by the vdW interactions,⁸⁸ as shown in **Figure 9**. Simulations also showed that the mechanical properties of such an entangled CNT network depend on the mass density of the system. However, such single zippering/unzippering mechanism is not enough to describe the frequency and density dependence on the viscoelasticity, as discussed below. More delicate simulation model is necessary, where other physical processes like sliding between CNTs, rotation and bending of CNTs, and bundling of CNTs should be included.⁸⁷

C. Densified CNT Assemblies

CNT films are more 2D-like than CNT gels which are mostly 3D assemblies. (CNT sheets are another 2D assembly, with a thickness less than tens to hundreds of nanometer, while CNT films usually refer to the assembly with a thickness over 1 μm .) The paper-like CNT films are also called buckypaper.^{54,79} Actually, it might be difficult to distinguish CNT films from CNT gels when their thicknesses are in the micrometer ranges. However, CNT films are often much more densified than CNT gels, and some films are just directly obtained by liquid densification on CNT gels. Therefore, the volumetric mass den-

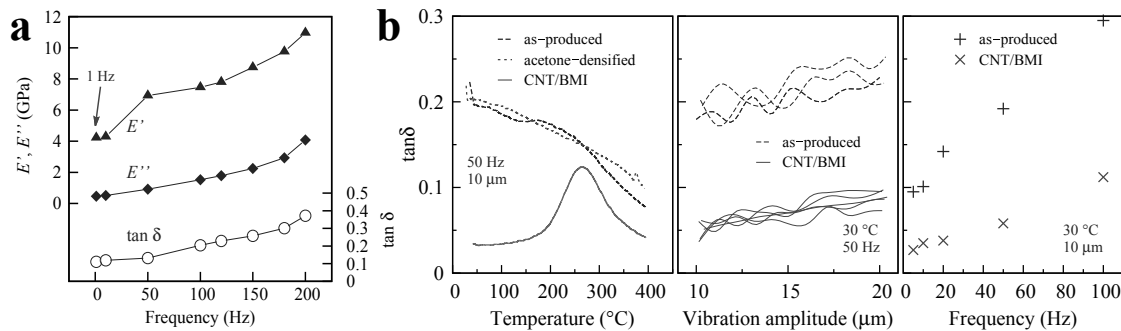


FIG. 10. (a) Dynamic mechanical properties (E' , E'' , and $\tan \delta$) of iCVD CNT films as functions of frequency.⁴⁹ (b) Loss tangent of various iCVD films as functions of temperature, vibration amplitude, and frequency, from tension-mode DMA tests.⁴⁴

sity is a nice criterion. For example, densities of 0.15–0.21 g cm⁻³,⁹¹ 0.26–0.42 g cm⁻³,⁷⁹ 0.47–0.51 g cm⁻³,⁴⁹ 0.54–0.62 g cm⁻³,⁵⁴ 0.50–0.85 g cm⁻³,³⁸ 0.84–1.04 g cm⁻³,³⁹ 1.21–1.35 g cm⁻³,^{38,40} and 0.81–1.39 g cm⁻³,⁹² have been reported recently. CNT films can also be used in sandwich beams to enhance the damping performance,⁹³ similar to the application of CNT forests.⁵¹

Although the CNTs are much more densified in these films, the entanglement feature of the CNTs is not different from the undensified gels.⁴⁴ Therefore, the vibration reduction ability can be quite similar to the gels except that the films also exhibit high modulus and strength. **Figure 10a** shows the dynamic properties of the iCVD films at different vibration frequencies, from the tension-mode DMA tests.⁴⁹ At a low frequency of 1 Hz, the loss tangent $\tan \delta$ was 0.11, smaller than the undensified gel ($\tan \delta \approx 0.3$ in a wide frequency range of 0.1–100 Hz),¹⁸ but much higher than many polymers whose Young's modulus is in the similar range of several GPa, see Figure 2. Interestingly, the damping ratio increases monotonically with frequency, nearly in a linear way, different from CNT gels. Furthermore, it is also surprising that the storage modulus E' could increase more than two-fold by increasing the frequency from <10 Hz to 200 Hz. Although the zipping/unzipping of CNT connection nodes and the sliding friction between CNTs were found to play roles here, there still should be some other issues to determine such frequency dependences in the damping ratio and storage modulus.

Besides the densification control, designing the intertube interactions is also efficient to tune the damping property. For another group of iCVD films, the as-produced film (pre-densified by ethanol) exhibited $\tan \delta \approx 0.1$ –0.3 in a frequency range of 5–100 Hz (Figure 10b),⁴⁴ higher than the previous report,⁴⁹ despite of the introduction of a post densification by acetone. As compared to the previous group of iCVD films, the CNTs here were less-walled (mainly double-walled) and the bundle size was also smaller (there was just about 50 tubes in a CNT bundle). We suspect that the number of CNT connection nodes could determine the damping performance at low frequencies, while the intertube interfaces

(contact areas) inside CNT bundles could be triggered to play roles with increasing the frequency.

Introducing polymers between CNTs is a widely used strategy to strengthen CNT assemblies.^{41–43,94} After the infiltration of BMI resins and post stretching and curing treatments, high strength CNT/BMI composite films can be obtained.⁴⁴ Although the strength and modulus were significantly increased for the composite film, the damping capacity was still non-negligible. For example, the loss tangent was still larger than 0.05 at 50 Hz. This means that the CNT-BMI interfaces and CNT-CNT contacts inside bundles still dissipate a certain vibration energy. Furthermore, the introduction of BMI caused the composite film to show a clear temperature dependence due to the glass transition (Figure 10b).

Figure 11 provides a direct comparison in loss tangent for different treatments on densified CNT networks, where dibutyl phthalate (DBP), tetraethyl orthosilicate (TEOS), poly(vinyl alcohol) (PVA), and phenol formaldehyde (PF) were infiltrated into CNT network (see Supporting Information for the infiltration details). Due to the different densification level, the original CNT film exhibited a loss tangent of 0.103, 0.136, and 0.208 at 20, 50, and 100 Hz, respectively, slightly smaller than that shown in Figure 10b. (Such difference could be ascribed to the different wall thickness of the CNTs, see Supporting Information.) After the DBP infiltration, the loss tangent was remarkably enhanced, up to 0.186, 0.238, and 0.310 at these frequencies. On the contrary, TEOS and PVA slightly reduced the damping performance, and the cured PF resulted in the smallest loss tangent (0.064, 0.078, and 0.130). Clearly, the polymer infiltration is an efficient way to tune the damping capacity, in a wide range that can reflect various materials in our daily life, such as nitrile butadiene rubber (NBR), latex film, polytetrafluoroethylene (PTFE) film, human hair, and laminating film (LF), see Figure 11b. (All the film samples were cut into a size of 15 mm × 0.5 mm, and tested in tensile mode DMA.)

The SEM characterization of the assembly structure provides evidences to understand the role of polymer infiltration (Figure S1, Supporting Information). DBP

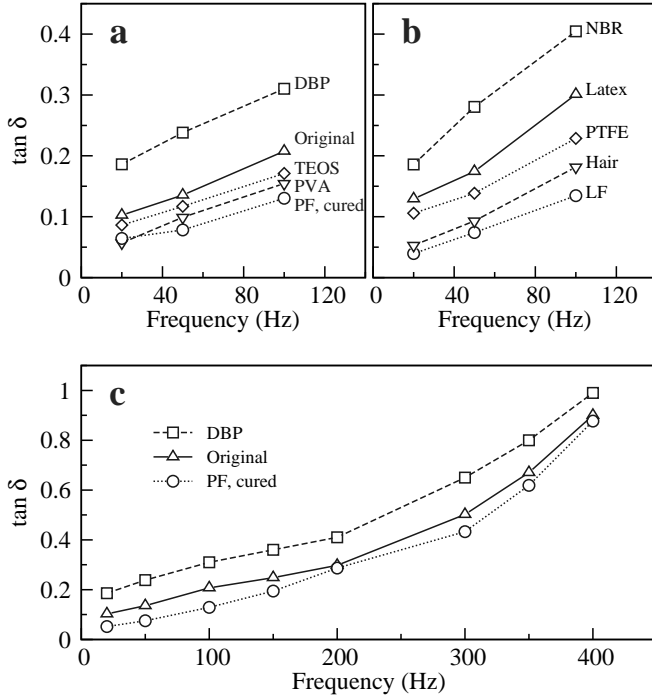


FIG. 11. Tuning the damping performance of CNT films by different organic compounds. (a) DBP infiltration can enhance the loss tangent, while other compounds suspend the damping performance. (b) The damping performance of various materials in our daily life. (c) A comparison between DPB-infiltrated, PF-infiltrated, and original CNT films in a wide range of frequency.

molecules can not only infiltrate into CNT bundles but also adhere the connection nodes. Such infiltration brings more viscous characteristics to CNT bundles and their connections, and thus improves greatly the damping performance. On the contrary, the cured PF network is rather much more rigid and elastic, and can store more energy as reflected by the reduced loss tangent.

Nevertheless, all these CNT films exhibited clear frequency dependence. By extending the vibration frequency up to 400 Hz, the loss tangent increased up to 0.900, 0.990, and 0.877 for the original, DBP-infiltrated, and PF-infiltrated films (Figure 11c). Such frequency-dependent energy dissipation is strongly related to the intrinsic viscosity of the constituents according to the Kelvin-Voigt model. This means that the simple zipping/unzipping behavior can not fully capture the dissipation mechanism. For example, the wall thickness of CNT was found to play interesting roles in the dynamic properties. Under the same iCVD process, the slight difference in growth condition could cause the tube's wall number to change from 2–3 to around 10.^{44,73,84,85} By testing the two different iCVD films, composed by the few-walled and multi-walled CNTs, a clear thickness dependence was observed. For example, the few-walled films exhibited a loss tangent of 0.327 at 200 Hz, while such value was just 0.207 for the multi-walled films (see

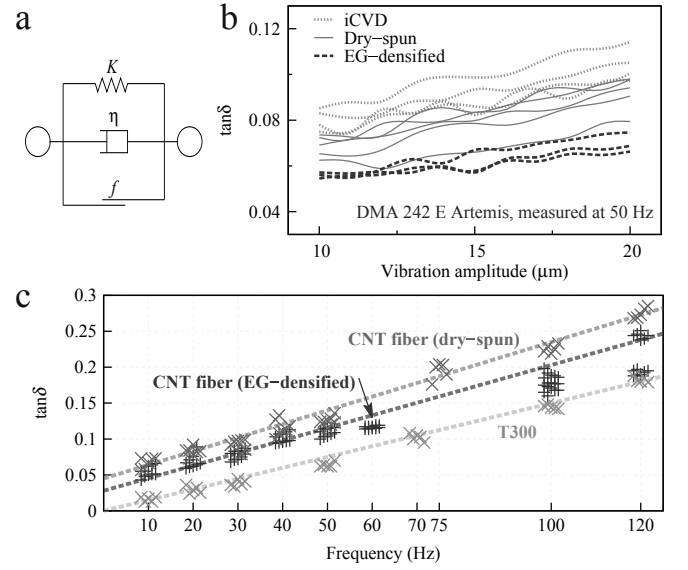


FIG. 12. Dynamic properties of CNT fibers.²¹ (a) Schematic of a modified Kelvin-Voigt model. (b) $\tan \delta$ increase slightly with vibration amplitude, for different CNT fibers. (c) The frequency dependence of $\tan \delta$ for CNT fibers, with a comparison to T300 carbon fiber.

Supporting Information for more details). We suspect that the wall thickness can affect the intrinsic viscosity of the CNT bundle and that the higher flexibility and bendability of few-walled CNTs can also induce energy dissipation during their structural deformation.

D. CNT Fibers

Vibration reduction of fiber-reinforced composites have been investigated for decades,^{6,8,35,95–97} and the filler-matrix interface or interphase region adjacent to fiber surface are found to effectively modify the viscoelastic nature of matrix, either increasing or decreasing. Different from traditional fibers which are usually a solid structure without internal interfaces, CNT fibers (indeed, not yarns) are a continuous length of interlocked nano-sized filaments of CNT bundles.²¹ As results, the interfacial properties between CNT fiber and polymer matrix can be totally different,^{98–100} and the fiber's vibrational mechanical property shows new features as compared with the traditional fibers.

Owing to the rich inter-filament contacts, the analysis of the dissipation mechanism for CNT fiber is quite reminiscent to the case of staple yarns.¹⁰² A modified Kelvin-Voigt model is used here, where a linear elastic spring K which stores energy (i.e., fiber's modulus E), an energy dissipation mechanism associated with the internal viscosity η of the filaments, and an energy dissipation mechanism of the coulomb form associated with the sum of inter-bundle friction f are connected in parallel (Figure 12a). One should notice that due to the hier-

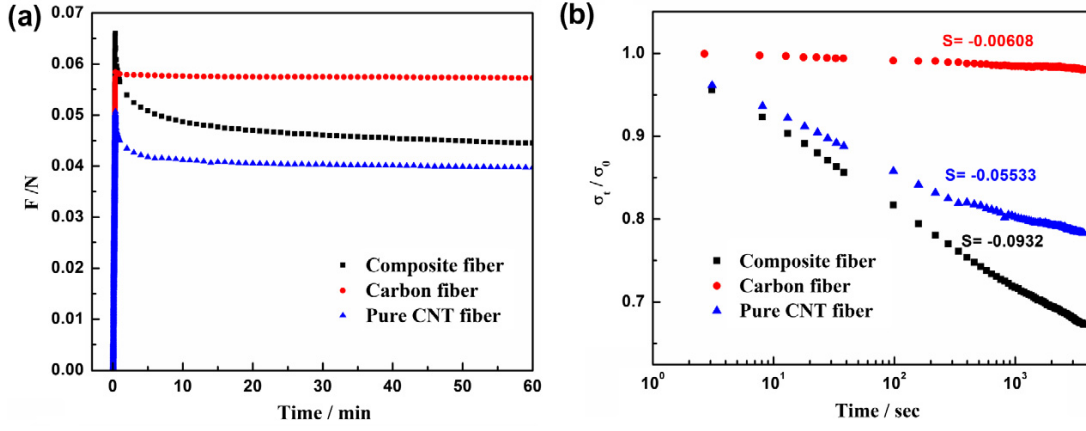


FIG. 13. Comparisons of relaxation behavior of carbon fiber, pure CNT fiber and CNT/epoxy composite fiber.¹⁰¹ (a) Force as a function of time during loading and relaxation. (b) Stress ratio σ_t/σ_0 as a function of time.

archical feature, η is also related to the intertube friction within a CNT bundle. According to this model, an effective damping coefficient $\eta^* = \eta + 4f/A\omega$ can be obtained, where A and ω are the vibration amplitude and frequency. Thus, the measured loss tangent contains frequency- and friction-dependent components, by $\tan \delta = \eta\omega/K + 4f/AK$.²¹

Figure 12b compares the loss tangent for different CNT fibers. The iCVD fiber showed the highest $\tan \delta$, even more than that of the dry-spun fiber (spun from CNT forests). This means, the dissipation by the CNT connection nodes might be missing in this modified Kelvin-Voigt model. Nevertheless, due to the high alignment of the CNTs, such model is very useful to understand the effects of densification and interfacial locking. As one can find from Figure 12b and c, the densified fibers by ethylene glycol (EG) exhibited the lower damping capacity, and the loss tangent generally increased with vibration amplitude and frequency, in agreement with the model analysis. Furthermore, the $\tan \delta$ - ω plots have revealed the main difference between CNT fiber and carbon fiber.

On one hand, the different $\tan \delta$ -to- ω slopes captured the difference in elastic modulus. The T300 carbon fiber had a modulus up to 204–238 GPa, while it was just 45–59 and 72–101 GPa for the dry-spun and EG-densified CNT fibers, respectively. On the other hand, the nonzero extrapolated $\tan \delta$ at $\omega = 0$ means that even without external vibrations, there is always energy loss at the CNT interfaces. For the dry-spun and EG-densified fibers, $\tan \delta|_{\omega=0} = 0.045$ and 0.028 , in agreement with the hysteresis test at 0.1 Hz where a dry-spun fiber exhibited a loss ratio of 0.05.¹⁰³ (Such ratio corresponded to the energy loss per stress-strain cycle, for example, of around 30%.⁵³) This difference reflected their different frictional feature in the assembly structures. After the densification, the improved packing density increased the inter-bundle contact area and enhanced the interfacial frictional force. However, the tendency of CNT slippage was thus remarkably suppressed. Therefore, f in the model

describes the level of overall frictional energy dissipation, reflecting not only the magnitude of frictional force but also the total number of interfaces where sliding phenomenon might take place.

The introduction of cross-linking BMI network in CNT fibers can strongly suspend the sliding energy dissipation, as reflected by the reduced loss tangent, which varied from 0.122 to 0.157 with an average of 0.136 at 100 Hz, in also agreement with the study on CNT/BMI composite films (Figure 10b).

According to such philosophy, the introduction of fiber-fiber contacts can increase the sliding dissipation. For example, by multi-plying CNT fibers together, a real CNT yarn can be obtained. Due to the increased inter-fiber contacts, a 400-ply CNT yarn showed a high loss tangent of $\tan \delta = 0.185$ at 10 Hz, under a linear mass density of 65 tex. Such value is already higher than the cotton yarns ($\tan \delta = 0.13$ – 0.176 at 10 Hz).

For CNT fibers and multi-ply CNT yarns, the creep, creep recovery and stress relaxation behaviors are also of great interests.^{53,101,104} For a two-ply CNT yarn, the stress relaxed no more than 15% when it was held for 20 h at 6% strain, and the majority of the stress relaxation occurred within the first 20 min.⁵³ For a pure CNT fiber, there was significant load decay during the first 4 min of the relaxation process, and the load dropped by $\sim 32\%$ after 18 h at constant strain.¹⁰¹ The CNT/epoxy composite fiber showed the similar relaxation behavior, while the load of the carbon fiber was almost constant after 1 h and decreased by only 5.4% even after 18 h (Figure 13a). This is because when a CNT fiber is held at a constant strain, slippage among CNT bundles within the fiber can take place, resulting in a gradual load drop. Figure 13b presents the stress relaxation plot of stress ratio, between the stress at a specific time σ_t and the maximum stress σ_0 , as a function of time for the three specimens. The stress relaxation rate of the composite fiber was higher than that of the pure fiber at the same initial strain level, even though the composite fiber re-

tained a higher load after 1 h. The possible mechanism could be the insufficient interaction between CNT and epoxy; the polymer induces high efficient load transfer between CNTs and thus improves the modulus, but the additional sliding at the CNT-epoxy interfaces could still occur during the relaxation process.

Differently, owing to the inter-fiber contacts, the multiply CNT yarns can show three distinct regions in the stress-strain relationship when subjected to monotonic tensile load.¹⁰⁴ Initially, the friction between CNT fibers does not allow significant slippage of the yarns. In the intermediate stage, CNT fibers slip relative to each other that results in the reduction of the helix angle up to a certain value. Thereafter in the third region, stretching of yarns occurs causing further tightening.

IV. DISCUSSION

The study on CNT-reinforced composites can cast lights on the analysis of CNT assemblies. In a recent study, to show the effect of inherent damping of matrix and interfacial slip, with minimizing other energy dissipation mechanisms, such as matrix tearing and plasticity, the CNTs were dominantly oriented parallel to the loading direction via hot-drawing.¹⁰⁵ In such CNT/PS composites, a “slip-stick” mechanism is found as the source for energy dissipation. At the CNT-polymer interface, debonding takes place upon a critical shear strain, and the initial bonds and interactions are broken. Broken covalent bonds are irreversible, whereas the mechanical interlocking and vdW interactions are reversible. Above the critical strain, when dynamic loading is applied, the interlocking and vdW interactions can be repeatedly reformed and broken, corresponding to stick and slip occurring at the interface.

However, the mechanisms for energy dissipation differ greatly from sample to sample, and also vary when the same sample is under different strains. For a CNT/epoxy composite containing $\sim 50\%$ volume fraction of CNTs,³¹ there is a critical threshold of shear strain of about 5%. When the strain is lower than the threshold, very few tube-tube contacts reach the critical stress for interfacial slip, and the energy loss is small. At the critical strain, intertube sliding is activated, particularly for CNT bundles closely aligned to the shear direction, and the damping shows a sharp increase. Peak damping is achieved for about 10% strain when most CNTs in the film will slip. The slight decrease of loss modulus at larger strains ($>10\%$) could be related to dynamic friction between the CNT shells of an MWCNT which is shown to be lower than static friction.

For CNT assemblies, the constituent nanotubes are built up by means of bundling, stacking, cross-linking, entangling, and possible intertube covalent bonding. The interfacial engineering obviously determines the statical and dynamical mechanical properties of the assembly materials.¹⁰⁶ By learning from the CNT-reinforced com-

posites, we suggest the following issues for future consideration:

(1) Connection nodes of nano-assemblies. The connection here is restricted to the contact between non-entangled CNTs (the entanglement is described below). The connection nodes are very essential to provide mechanical support for CNT gels, sponges, and buckypapers. Zipping and unzipping at the nodes, usually the contacts of non-entangled CNTs,⁴⁰ have been considered to contribute mostly the viscoelasticity. Welding these nodes, including graphene coating,⁷¹ deposition of amorphous carbon,⁷³ and strapping with long-chain polymers,⁸⁴ can suspend the zipping/unzipping and thus improve the elasticity or allow super-high stretchability. For future development, strategies to enhance the node’s damping capacity are still of great importance. The design of CNT-polymer connection nodes is also helpful to introduce more damping ways.

(2) Entanglement of CNTs. Entanglement is another assembly parameter, and does also result in connection nodes in CNT networks, but such nodes do not show zipping/unzipping but a “stick-slip” sliding motion upon stretching or compressing.^{107,108} The entanglement also causes self-folding of two intersecting CNTs and the intersecting point transfers load from one CNT to the other.¹⁰⁹ Due to such “intersecting” entanglement, CNT network shows also high viscoelasticity⁴⁹ and is highly stretchable.^{44,84} Notice that, in many studies of the iCVD CNT assemblies,^{44,49,73,84} the “intersecting” entanglement and “non-entangled” contact co-exist, but unfortunately many previous studies just payed attention to the latter one.

(3) Intertube covalent and non-covalent interactions. This is an interfacial point of view. The covalent bonding benefits the load transfer between CNTs, especially for highly aligned tubes. The similar treatment is the introduction of cross-linked polymer network inside the aligned CNTs. These treatments make as many as the CNTs response simultaneously to strains,^{110,111} resulting in significant improvement in material’s modulus. However, the tendency of sliding between CNTs is suspended, reducing the frictional energy dissipation.²¹ Therefore, a certain level of non-bonded CNT contacts is still welcome towards high viscoelastic assemblies.

(4) Inherent viscoelasticity of CNT and CNT bundles, the basic components of the assembly. Although CNT is a super-elastic material with a modulus up to TPa scale, it can still cost energy by structural deformation such as buckling and collapsing. Thus, the tube itself can exhibit inherent viscoelasticity in some cases like the compression on CNT forests.^{22,46,48,112} Thus, there could be a strategy to make CNT assemblies more viscoelastic by modifying the nanotube structure, e.g., introduction of defects that cause more dissipation under interfacial sliding, changing straight tube structure into helical,^{113,114} and so on.

From the development, a new stiffness (modulus)-loss map for CNT assembly materials is provided in **Figure 14**. So far, there are just countable studies on CNT as-

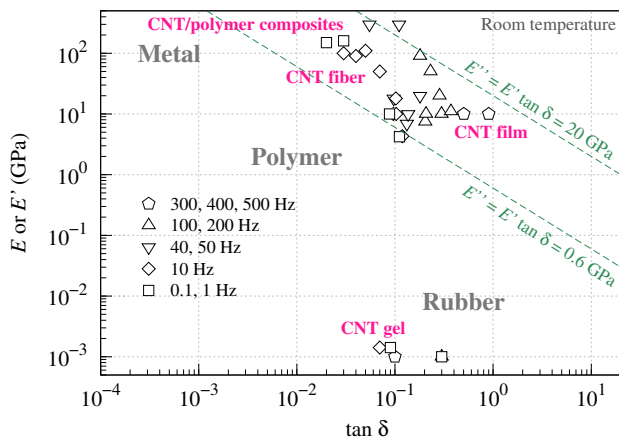


FIG. 14. Modulus-loss map for CNT assembly materials. The Young's modulus E and storage modulus E' are mixed as they are collected from different literature and the present study. These CNT materials are CNT/BMI and CNT/polyimide composite films,^{44,94} CNT films densified from CNT gels^{44,49} and stacked-up using CNT sheets,⁴⁰ CNT fibers,²¹ CNT gels,^{18,71,73} and high-density CNT forests.⁴⁶ The two reference lines represent $E'' = E' \tan \delta = 0.6$ GPa and 20 GPa, respectively.

assembly materials. However, due to the rich interfacial areas between CNTs and between CNT and polymers, a high loss tangent can be realized at a high storage modulus. For most materials, even practical polymer damping layers, $E' \tan \delta$ is less than 0.6 GPa (Figure 2), while for CNT assemblies, the upper limit of $E' \tan \delta$ could be about 20 GPa. Clearly, such performance is a big step towards the “best performance”, and such performance can only be observed in some extreme viscoelastic metals and composites.¹¹⁵

Figure 14 also demonstrates an interesting phenomenon, that with densifying CNT gels into films, the modulus increases by orders of magnitude while the loss tangent could be uninfluenced. As the CNT connection nodes, intertube interaction, CNT alignment, and entanglement are totally different, the major contribution to the viscoelasticity should also vary greatly. Therefore, we still should pay great efforts to CNT assembly materials.

V. CONCLUSION

We have introduced basic concepts of viscoelasticity and discussed recent progresses on the dynamic properties of CNT assembly materials. Due to the rich intertube contacts and various ways to dissipate energy, CNT assemblies have shown great advantages for developing novel high-damping materials, which can also show high strength or modulus for engineering applications. Towards future development of such multifunctional assembly materials, the design and control of interface structure, interactions, and connection ways between CNTs

are still the key problems.

ACKNOWLEDGMENTS

We thank financial supports from the National Natural Science Foundation of China (51561145008, 21503267, 11302241, 11404371, 21473238), Youth Innovation Promotion Association of the Chinese Academy of Sciences (2015256), and National Key Research and Development Program of China (2016YFA0203301).

¹D. D. L. Chung, J. Mater. Sci. **36**, 5733 (2001).

²R. S. Lakes, J. Compos. Mater. **36**, 287 (2002).

³J. Luo, Z. Duan, G. Xian, Q. Li, and T. Zhao, Mech. Adv. Mater. Struct. **22**, 224 (2015).

⁴X. Q. Zhou, D. Y. Yu, X. Y. Shao, S. Q. Zhang, and S. Wang, Compos. Struct. **136**, 460 (2016).

⁵D. D. L. Chung, J. Alloys Compd. **355**, 216 (2003).

⁶R. Chandra, S. P. Singh, and K. Gupta, Compos. Struct. **46**, 41 (1999).

⁷S. U. Khan, C. Y. Li, N. A. Siddiqui, and J.-K. Kim, Compos. Sci. Technol. **71**, 1486 (2011).

⁸K. S. Kumar, I. Siva, P. Jeyaraj, J. T. W. Jappes, S. C. Amico, and N. Rajini, Mater. Des. **56**, 379 (2014).

⁹P. Zhang, M. A. Heyne, and A. C. To, J. Mech. Phys. Solids **83**, 285 (2015).

¹⁰L. Liu, W. Ma, and Z. Zhang, Small **7**, 1504 (2011).

¹¹W. Lu, M. Zu, J.-H. Byun, B.-S. Kim, and T.-W. Chou, Adv. Mater. **24**, 1805 (2012).

¹²Y. Liu and S. Kumar, ACS Appl. Mater. Interfaces **6**, 6069 (2014).

¹³J. Di, X. Zhang, Z. Yong, Y. Zhang, D. Li, R. Li, and Q. Li, Adv. Mater. **28**, 10529 (2016).

¹⁴X. Zhang, X. Yu, J. Zhao, and Q. Li, in *Carbon Nanotubes - Current Progress of their Polymer Composites*, edited by M. R. Berber and I. H. Hafez (InTech - Open Access, Rijeka, Croatia, 2016) Chap. 3, pp. 73–93.

¹⁵D. P. Hashim, N. T. Narayanan, J. M. Romo-Herrera, D. A. Cullen, M. G. Hahm, P. Lezzi, J. R. Suttle, D. Kelkhoff, E. Muñoz Sandoval, S. Ganguli, A. K. Roy, D. J. Smith, R. Vajtai, B. G. Sumpter, V. Meunier, H. Terrones, M. Terrones, and P. M. Ajayan, Sci. Rep. **2**, 363 (2012).

¹⁶Z. Lin, Z. Zeng, X. Gui, Z. Tang, M. Zou, and A. Cao, Adv. Energy Mater. **6**, 1600554 (2016).

¹⁷A. Cao, P. L. Dickrell, W. G. Sawyer, M. N. Ghasemi-Nejhad, and P. M. Ajayan, Science **310**, 1307 (2005).

¹⁸M. Xu, D. N. Futaba, T. Yamada, M. Yumura, and K. Hata, Science **330**, 1364 (2010).

¹⁹C. Wang, B. Xie, Y. Liu, and Z. Xu, ACS Macro Lett. **1**, 1176 (2012).

²⁰Y. Won, Y. Gao, M. A. Panzer, R. Xiang, S. Maruyama, T. W. Kenny, W. Cai, and K. E. Goodson, Proc. Natl. Acad. Sci. **110**, 20426 (2013).

²¹J. Zhao, X. Zhang, Z. Pan, and Q. Li, Adv. Mater. Interfaces **2**, 1500093 (2015).

²²Y. Li, H.-i. Kim, B. Wei, J. Kang, J.-b. Choi, J.-D. Nam, and J. Suhr, Nanoscale **7**, 14299 (2015).

²³Z. Shen, M. Röding, M. Kröger, and Y. Li, Polymers **9**, 115 (2017).

²⁴J. D. Ferry, *Viscoelastic Properties of Polymers*, 3rd ed. (John Wiley & Sons, New York, 1980).

²⁵M. A. Meyers and K. K. Chawla, *Mechanical Behavior of Materials*, 2nd ed. (Cambridge University Press, New York, 2009).

²⁶R. Lakes, *Viscoelastic Materials* (Cambridge University Press, New York, 2009).

- ²⁷J. Lemaitre, in *Handbook of Materials Behavior Models*, edited by J. Lemaitre (Academic Press, San Diego, USA, 2001) Chap. 2.1, pp. 71–74.
- ²⁸P. J. Achorn and R. G. Ferrillo, *J. Appl. Polym. Sci.* **54**, 2033 (1994).
- ²⁹J. Suhr, W. Zhang, P. M. Ajayan, and N. A. Koratkar, *Nano Lett.* **6**, 219 (2006).
- ³⁰X. Zhou, E. Shin, K. W. Wang, and C. E. Bakis, *Compos. Sci. Technol.* **64**, 2425 (2004).
- ³¹J. Suhr, N. Koratkar, P. Keblinski, and P. Ajayan, *Nat. Mater.* **4**, 134 (2005).
- ³²P. M. Ajayan, J. Suhr, and N. Koratkar, *J. Mater. Sci.* **41**, 7824 (2006).
- ³³Z. Wang, R. L. D. Whitby, M. Rousseau, S. Nevill, G. Geaves, and S. V. Mikhalevsky, *J. Mater. Chem.* **21**, 4150 (2011).
- ³⁴R. Agrawal, A. Nieto, H. Chen, M. Mora, and A. Agarwal, *ACS Appl. Mater. Interfaces* **5**, 12052 (2013).
- ³⁵D. Carponcin, E. Dantras, G. Michon, J. Dandurand, G. Aridon, F. Levallois, L. Cadiergues, and C. Lacabanne, *J. Non-Cryst. Solids* **409**, 20 (2015).
- ³⁶Y.-C. Chu, M.-H. Weng, W.-Y. Lin, H.-J. Tsai, and W.-K. Hsu, *RSC Adv.* **6**, 21271 (2016).
- ³⁷M. Eftekhari and A. Fatemi, *Int. J. Fatigue* **87**, 153 (2016).
- ³⁸Y. Wang, M. Li, Y. Gu, X. Zhang, S. Wang, Q. Li, and Z. Zhang, *Nanoscale* **7**, 3060 (2015).
- ³⁹L. Zhang, X. Wang, W. Xu, Y. Zhang, Q. Li, P. D. Bradford, and Y. Zhu, *Small* **11**, 3830 (2015).
- ⁴⁰X. Yu, X. Zhang, J. Zou, Z. Lan, C. Jiang, J. Zhao, D. Zhang, M. Miao, and Q. Li, *Adv. Mater. Interfaces* **3**, 1600352 (2016).
- ⁴¹Q. Cheng, J. Bao, J. Park, Z. Liang, C. Zhang, and B. Wang, *Adv. Funct. Mater.* **19**, 3219 (2009).
- ⁴²Q. Cheng, B. Wang, C. Zhang, and Z. Liang, *Small* **6**, 763 (2010).
- ⁴³X. Wang, Z. Z. Yong, Q. W. Li, P. D. Bradford, W. Liu, D. S. Tucker, W. Cai, H. Wang, F. G. Yuan, and Y. T. Zhu, *Mater. Res. Lett.* **1**, 19 (2013).
- ⁴⁴Y. Han, X. Zhang, X. Yu, J. Zhao, S. Li, F. Liu, P. Gao, Y. Zhang, T. Zhao, and Q. Li, *Sci. Rep.* **5**, 11533 (2015).
- ⁴⁵N. A. Koratkar, B. Wei, and P. M. Ajayan, *Compos. Sci. Technol.* **63**, 1525 (2003).
- ⁴⁶S. Pathak, Z. G. Cambaz, S. R. Kalidindi, J. G. Swadener, and Y. Gogotsi, *Carbon* **47**, 1969 (2009).
- ⁴⁷Q. Zhang, Y. C. Lu, F. Du, L. Dai, J. Baur, and D. C. Foster, *J. Phys. D: Appl. Phys.* **43**, 315401 (2010).
- ⁴⁸P. D. Bradford, X. Wang, H. Zhao, and Y. T. Zhu, *Carbon* **49**, 2834 (2011).
- ⁴⁹Q. Liu, M. Li, Y. Gu, S. Wang, Y. Zhang, Q. Li, L. Gao, and Z. Zhang, *Carbon* **86**, 46 (2015).
- ⁵⁰Y. Li and M. Kröger, *Soft Matter* **8**, 7822 (2012).
- ⁵¹N. Koratkar, B. Wei, and P. M. Ajayan, *Adv. Mater.* **14**, 997 (2002).
- ⁵²S. Fan, M. G. Chapline, N. R. Franklin, T. W. Tomblar, A. M. Cassell, and H. Dai, *Science* **283**, 512 (1999).
- ⁵³M. Zhang, K. R. Atkinson, and R. H. Baughman, *Science* **306**, 1358 (2004).
- ⁵⁴D. Wang, P. Song, C. Liu, W. Wu, and S. Fan, *Nanotechnology* **19**, 075609 (2008).
- ⁵⁵K. Mizuno, J. Ishii, H. Kishida, Y. Hayamizu, S. Yasuda, D. N. Futaba, M. Yumura, and K. Hata, *Proc. Natl. Acad. Sci.* **106**, 6044 (2009).
- ⁵⁶C. Fang, J. Zhao, J. Jia, Z. Zhang, X. Zhang, and Q. Li, *Appl. Phys. Lett.* **97**, 181906 (2010).
- ⁵⁷J. Jia, J. Zhao, G. Xu, J. Di, Z. Yong, Y. Tao, C. Fang, Z. Zhang, X. Zhang, L. Zheng, and Q. Li, *Carbon* **49**, 1333 (2011).
- ⁵⁸E. S. Polsen, M. Bedewy, and A. J. Hart, *Small* **9**, 2564 (2013).
- ⁵⁹K. Eom, K. Nam, H. Jung, P. Kim, M. S. Strano, J.-H. Han, and T. Kwon, *Carbon* **65**, 305 (2013).
- ⁶⁰Y. Zeng, L. Ci, B. J. Carey, R. Vajtai, and P. M. Ajayan, *ACS Nano* **4**, 6798 (2010).
- ⁶¹P. R. Mantena, T. Tadepalli, B. Pramanik, V. M. Boddu, M. W. Brenner, L. D. Stephenson, and A. Kumar, *J. Nanomater.* **2013**, 259458 (2013).
- ⁶²V. P. Veedu, A. Cao, X. Li, K. Ma, C. Soldano, S. Kar, P. M. Ajayan, and M. N. Ghasemi-Nejhad, *Nat. Mater.* **5**, 457 (2006).
- ⁶³K. Kim, P. R. Mantena, S. S. Daryadel, V. M. Boddu, M. W. Brenner, and J. S. Patel, *J. Nanomater.* **2015**, 480549 (2015).
- ⁶⁴V. M. Boddu and M. W. Brenner, *Appl. Phys. A* **122**, 88 (2016).
- ⁶⁵E. H. T. Teo, W. K. P. Yung, D. H. C. Chua, and B. K. Tay, *Adv. Mater.* **19**, 2941 (2007).
- ⁶⁶G. G. Silva, M.-T. F. Rodrigues, C. Fantini, R. S. Borges, M. A. Pimenta, B. J. Carey, L. Ci, and P. M. Ajayan, *Macromol. Mater. Eng.* **296**, 53 (2011).
- ⁶⁷D. Ürk, E. Demir, O. Bulut, D. Çakıroğlu, F. Ç. Cebeci, M. L. Öveçoğlu, and H. Cebeci, *Compos. Struct.* **155**, 255 (2016).
- ⁶⁸M. Xu, D. N. Futaba, M. Yumura, and K. Hata, *Adv. Mater.* **23**, 3686 (2011).
- ⁶⁹M. Xu, D. N. Futaba, M. Yumura, and K. Hata, *Nano Lett.* **11**, 3279 (2011).
- ⁷⁰X. Gui, J. Wei, K. Wang, A. Cao, H. Zhu, Y. Jia, Q. Shu, and D. Wu, *Adv. Mater.* **22**, 617 (2010).
- ⁷¹K. H. Kim, Y. Oh, and M. F. Islam, *Nat. Nanotechnol.* **7**, 562 (2012).
- ⁷²Z. Dai, L. Liu, X. Qi, J. Kuang, Y. Wei, H. Zhu, and Z. Zhang, *Sci. Rep.* **6**, 18930 (2016).
- ⁷³H. Wang, W. Lu, J. Di, D. Li, X. Zhang, M. Li, Z. Zhang, L. Zheng, and Q. Li, *Adv. Funct. Mater.* **27**, 1606220 (2017).
- ⁷⁴L. A. Hough, M. F. Islam, B. Hammouda, A. G. Yodh, and P. A. Heiney, *Nano Lett.* **6**, 313 (2006).
- ⁷⁵M. B. Brynning, D. E. Milkie, M. F. Islam, L. A. Hough, J. M. Kikkawa, and A. G. Yodh, *Adv. Mater.* **19**, 661 (2007).
- ⁷⁶J. Zou, J. Liu, A. S. Karakoti, A. Kumar, D. Joung, Q. Li, S. I. Khondaker, S. Seal, and L. Zhai, *ACS Nano* **4**, 7293 (2010).
- ⁷⁷K. H. Kim, M. Vural, and M. F. Islam, *Adv. Mater.* **23**, 2865 (2011).
- ⁷⁸S. Faraji, K. L. Stano, O. Yildiz, A. Li, Y. Zhu, and P. D. Bradford, *Nanoscale* **7**, 17038 (2015).
- ⁷⁹R. L. D. Whitby, T. Fukuda, T. Maekawa, S. L. James, and S. V. Mikhalevsky, *Carbon* **46**, 949 (2008).
- ⁸⁰R. L. D. Whitby, T. Fukuda, T. Maekawa, S. V. Mikhalevsky, and A. B. Cundy, *Nanotechnology* **21**, 075707 (2010).
- ⁸¹K. H. Kim, M. N. Tsui, and M. F. Islam, *Chem. Mater.* **29**, 2748 (2017).
- ⁸²Y.-L. Li, I. A. Kinloch, and A. H. Windle, *Science* **304**, 276 (2004).
- ⁸³M. Motta, Y.-L. Li, I. Kinloch, and A. Windle, *Nano Lett.* **5**, 1529 (2005).
- ⁸⁴J. Zou, X. Zhang, J. Zhao, C. Lei, Y. Zhao, Y. Zhu, and Q. Li, *Compos. Sci. Technol.* **135**, 123 (2016).
- ⁸⁵J. Zou, X. Zhang, C. Xu, J. Zhao, Y. T. Zhu, and Q. Li, *Carbon* **121**, 242 (2017).
- ⁸⁶S. W. Cranford and M. J. Buehler, *Nanotechnology* **21**, 265706 (2010).
- ⁸⁷B. Xie, Y. Liu, Y. Ding, Q. Zheng, and Z. Xu, *Soft Matter* **7**, 10039 (2011).
- ⁸⁸X. Yang, P. He, and H. Gao, *Nano Res.* **4**, 1191 (2011).
- ⁸⁹Y. Li and M. Kröger, *Carbon* **50**, 1793 (2012).
- ⁹⁰H. Chen, L. Zhang, J. Chen, M. Becton, X. Wang, and H. Nie, *Carbon* **109**, 19 (2016).
- ⁹¹R. Thevamaran, D. Saini, M. Karakaya, J. Zhu, R. Podila, A. M. Rao, and C. Daraio, *Nanotechnology* **28**, 184002 (2017).
- ⁹²L. Zhang, G. Zhang, C. Liu, and S. Fan, *Nano Lett.* **12**, 4848 (2012).
- ⁹³Y. Ji, Y.-J. Lin, and J. S. C. Wong, in *2006 1st IEEE International Conference on Nano/Micro Engineered and Molecular Systems* (Zhuhai, China, 2006) pp. 725–729.
- ⁹⁴D. Hu, Y. Xing, M. Chen, B. Gu, B. Sun, and Q. Li, *Compos. Sci. Technol.* **141**, 137 (2017).
- ⁹⁵R. F. Gibson and R. Plunkett, *J. Compos. Mater.* **10**, 325 (1976).

- ⁹⁶K. E. Reed, Polym. Compos. **1**, 44 (1980).
- ⁹⁷L. Uma Devi, S. S. Bhagawan, and S. Thomas, J. Appl. Polym. Sci. **64**, 1739 (1997).
- ⁹⁸M. Zu, Q. Li, Y. Zhu, M. Dey, G. Wang, W. Lu, J. M. Deitzel, J. W. Gillespie, J.-H. Byun, and T.-W. Chou, Carbon **50**, 1271 (2012).
- ⁹⁹Y.-N. Liu, M. Li, Y. Gu, X. Zhang, J. Zhao, Q. Li, and Z. Zhang, Carbon **52**, 550 (2013).
- ¹⁰⁰C. Lei, J. Zhao, J. Zou, C. Jiang, M. Li, X. Zhang, Z. Zhang, and Q. Li, Adv. Eng. Mater. **18**, 839 (2016).
- ¹⁰¹M. Zu, Q. Li, Y. Zhu, Y. Zhu, G. Wang, J.-H. Byun, and T.-W. Chou, Carbon **52**, 347 (2013).
- ¹⁰²T. Murayama, J. Appl. Polym. Sci. **24**, 1413 (1979).
- ¹⁰³A. Hehr, M. Schulz, V. Shanov, and A. Song, J. Intell. Mater. Syst. Struct. **25**, 713 (2014).
- ¹⁰⁴H. E. Misak, V. Sabelkin, L. Miller, R. Asmatulu, and S. Mall, J. Nanosci. Nanotechnol. **13**, 8331 (2013).
- ¹⁰⁵F. Gardea, B. Glaz, J. Riddick, D. C. Lagoudas, and M. Naraghi, ACS Appl. Mater. Interfaces **7**, 9725 (2015).
- ¹⁰⁶X. Zhang, in *Nanomechanics*, edited by A. Vakhrushev (InTech - Open Access, Rijeka, Croatia, 2017) Chap. 1, pp. 1–29.
- ¹⁰⁷B. Bhushan, X. Ling, A. Jungen, and C. Hierold, Phys. Rev. B **77**, 165428 (2008).
- ¹⁰⁸B. Bhushan and X. Ling, Phys. Rev. B **78**, 045429 (2008).
- ¹⁰⁹W. Lu and T.-W. Chou, J. Mech. Phys. Solids **59**, 511 (2011).
- ¹¹⁰A. Kis, G. Csányi, J.-P. Salvetat, T.-N. Lee, E. Couteau, A. J. Kulik, W. Benoit, J. Brugger, and L. Forró, Nat. Mater. **3**, 153 (2004).
- ¹¹¹W. Ma, L. Liu, Z. Zhang, R. Yang, G. Liu, T. Zhang, X. An, X. Yi, Y. Ren, Z. Niu, J. Li, H. Dong, W. Zhou, P. M. Ajayan, and S. Xie, Nano Lett. **9**, 2855 (2009).
- ¹¹²C. Cao, A. Reiner, C. Chung, S.-H. Chang, I. Kao, R. V. Kukta, and C. S. Korach, Carbon **49**, 3190 (2011).
- ¹¹³Q. Zhang, M.-Q. Zhao, D.-M. Tang, F. Li, J.-Q. Huang, B. Liu, W.-C. Zhu, Y.-H. Zhang, and F. Wei, Angew. Chem. Int. Ed. **49**, 3642 (2010).
- ¹¹⁴M.-Q. Zhao, Q. Zhang, G.-L. Tian, J.-Q. Huang, and F. Wei, ACS Nano **6**, 4520 (2012).
- ¹¹⁵Y. C. Wang, M. Ludwigson, and R. S. Lakes, Mater. Sci. Eng. A **370**, 41 (2004).

Supporting Information

In this supporting information, the synthesis details and characterization results are provided to support the discussion in Sec. IIIC. These results were for the CNT/DBP, CNT/TEOS, CNT/PVA, and CNT/PF composite films, as compared to the untreated iCVD films. For the iCVD films, under the similar assembly structure, there was also evidences to show the effect of tube structure on the film's damping performance.

The reference numbers here are the same as in the main text.

Fabrication of iCVD films: For the CNT growth, a tube furnace was heated up to 1300 °C with a heating rate of 10 °C/min in Ar atmosphere. Then, a solution of ethyl alcohol with 1.2 vol% ferrocene and 0.4 vol% thiophene was injected at a rate of 20 mL h⁻¹ into the furnace, carried by an Ar/H₂ gas mixture.⁷³ Such group of growth parameters is different from our previous attempt where ethanol was the carbon source and the ferrocene and thiophene contents were 2 wt% and 1 vol%.^{44,84,85} As a result, the present CNTs were mainly multi-walled,⁷³ while the previous result showed a large amount of double- and triple-walled CNTs were observed.^{44,84,85}

The as-grown CNTs, highly entangled due to the gas flow, were collected layer-by-layer on a rotating mandrel (diameter 400 mm). A gel structure was obtained by the direct winding, and a simultaneous spraying of liquid (mostly ethanol) during the winding could produce the densified CNT films.

Effect of tube thickness on damping performance: As we have provided in the main text, the wall thickness has shown clear influence on the loss tangent. **Table S1** shows a comparison of loss tangent between two different iCVD films. At the similar bundle size of ~50 nm, the wall thickness can greatly affect the intrinsic viscosity of the CNT bundle. First, the less wall number, the smaller tube diameter, and thus the larger contact area between CNTs in the bundle. Second, the few-walled CNTs are generally much softer than the multi-walled tubes, in flexibility and bendability. These features can easily induce intertube sliding and structural deformation, resulting in the increase in loss tangent.

Preparation of CNT composite films: The as-produced ethanol-densified iCVD films were post treated in the following ways. (1) Infiltration of DBP or TEOS: After being soaked in DBP or TEOS liquid for 8 h, the CNT/DBP or CNT/TEOS composite film was compressed with a compression roller at 150 °C, below the boiling point of the organics. (2) Infiltration of PVA: The 8-h soaking was performed in a 0.5 wt% PVA/water solution. After the soaking, the film was dried at 80 °C for 3 h, and then compressed. (3) Infiltration and curing of PF: The solution was a 13.7 wt% PF resin/acetone solution. After the 8-h soaking, the film was washed by acetone and dried naturally. The curing was performed at 10 MPa and 150 °C for 5 min. (4) The control sample

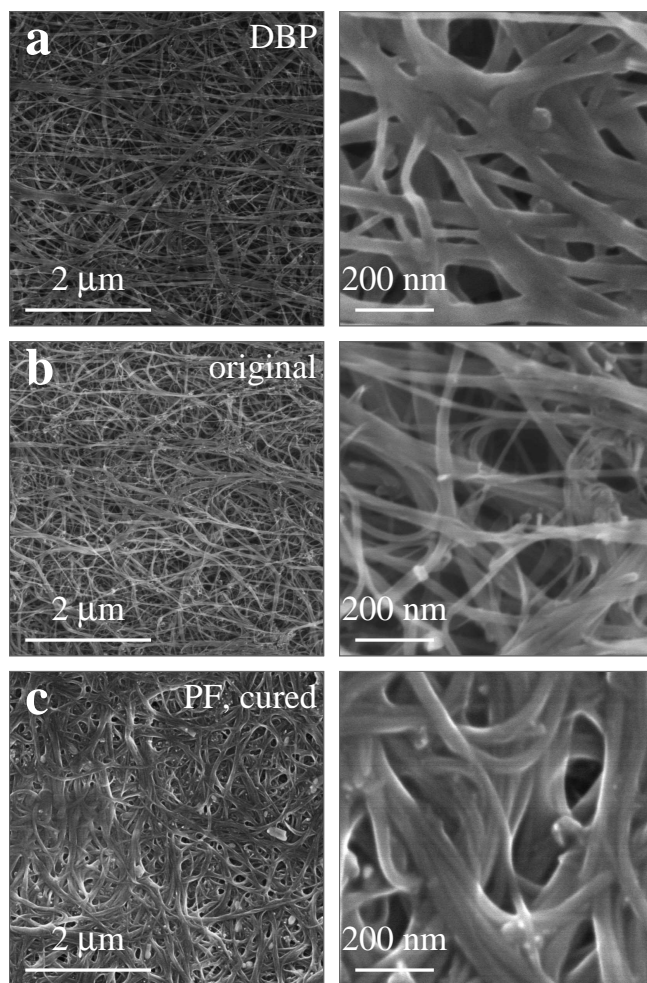


FIG. S1. Assembly morphologies of the CNT/DBP, pure CNT (iCVD), and CNT/PF films.

of iCVD film was also compressed with a compression roller, in order to obtain the similar CNT packing density for all samples.

Polymer-tuned intertube contacts: **Figure S1** compares the assembly morphologies of the CNT/DBP, pure CNT (iCVD), and CNT/PF films. The lower magnification results (left panels) show clearly that the CNTs were packed together under a similar density. However, the amount of infiltrated organic compounds were different due to the different molecular weights. There was about 11–14 wt% infiltration of DBP according to thermogravimetry (divided by the total mass of the composite film), and the infiltration was much larger for PF, about 28–33 wt%.

The higher magnification results (right panels in Figure S1) show totally different intertube contacts in these films. The infiltrated DBP molecules mostly locate inside the CNT bundles and/or around the connection nodes of the bundles. However, the overall CNT network seems to be as similar as to the original sample. Due to the viscosity of DBP, both the intrinsic viscosity of CNT

TABLE S1. A comparison of loss tangent between two different iCVD films, which were composed by few-walled and multi-walled CNTs, respectively.

Wall number	Bundle size (nm)	Frequency (Hz)						Reference
		1	10	20	50	100	200	
2-3	~50		0.101	0.142	0.192	0.295		Sci. Rep. 2015 ⁴⁴
2-3	~50		0.119		0.132	0.204	0.372	Carbon 2015 ⁴⁹
~10		0.090						AFM 2017 ⁷³
~10	~50	0.088	0.096	0.103	0.136	0.207	0.298	this study

bundle and the zipping/unzipping behavior at the connection nodes could induce more energy dissipation, as reflected in the increase in loss tangent. For the CNT/PF composite film, although the polymer fraction was much higher, the cured polymer network is indeed an elastic material. This phenomenon can not only hinder the zipping/unzipping behavior, but also increase the elasticity of CNT bundle. Therefore, the CNT/PF composite film exhibited the lowest loss tangent.

Testing methods: A T150 Universal Testing Machine (Keysight Technologies, Inc., Santa Rosa, USA) and a DMA 242 E Artemis (NETZSCH-Gerätebau GmbH, Selb, Germany) were used to characterize the

dynamic properties. Frequencies ranging from 10 to 400 Hz were used in the T150 system, and 1 to 100 Hz in the DMA 242 E Artemis. The two testers provided the same results for the testings at the frequencies.²¹ The vibration amplitude was controlled as load force variation and displacement variation in the two tester, respectively. For the T150 system, the default value of $A_f = 4.5$ mN for the force variation corresponded to a displacement amplitude (A) of several m for a given gauge length L , modulus E , and cross sectional area S , by $A_f/SE = A/L$.²¹ For the tests with DMA 242 E Artemis, 10 μm was used for the displacement amplitude.